Trans Indian Inst Met (2016) 69(2):223–227
DOI 10.1007/s12666-015-0757-8

TECHNICAL PAPER

# Origin of Threshold Stresses in a P92-type Steel

**V. Dudko**[1] · **A. Belyakov**[1] · **R. Kaibyshev**[1]

Received: 8 October 2015 / Accepted: 11 November 2015 / Published online: 15 December 2015
© The Indian Institute of Metals - IIM 2015

**Abstract** The creep behavior of a P92-type steel was examined at 923 K. The threshold shear stress of 51 MPa was revealed by an analysis of steady state creep behavior at applied stress ranging from 118 to 200 MPa. The tempered martensite lath structure stabilized by $M_{23}C_6$-type carbide particles with an average size of about 110 nm and MX-type carbonitrides with a size of 40 nm located within ferritic matrix evolved after tempering. The transient creep at an applied stress of 118 MPa was accompanied by two-fold decrease in internal elastic stress and dislocation density. The threshold stresses matched the values of internal stresses, which were measured by means of the lattice curvature within individual laths, and those corresponded to Orowan stressor detachment stress originated from M(C,N) carbonitrides. A dispersion of M(C,N) carbonitrides played a crucial role in superior creep resistance of P92-type steels because of dispersion hardening and hindering the relief of internal stresses originated from lath boundaries.

**Keywords** Creep · Threshold stress · Internal stress · Microstructure

## 1 Introduction

9 %Cr martensitic steels such as P92 are used for high-temperature components of fossil power plants. Superior creep resistance of this steel is provided by combination of solute hardening, precipitation hardening and substructure/deformation hardening, which are generally considered as primary strengthening mechanisms responsible for creep resistance [1, 2]. Substitutional solute atoms, such as Mo and W, which are much larger than the solvent iron, are used as effective solid solution strengtheners [2]. Alloying with Nb and V causes dispersion strengthening originated from nanoscale Nb- and V-rich M(C,N) carbonitrides, which precipitated at dislocations within the laths of tempered martensite [2–4]. The substructure/deformation hardening is attributed to the lath structure containing a high dislocation density. The $M_{23}C_6$-type carbides stabilize tempered lath martensite structure (TMLS) under creep conditions until the end of the steady state creep [2, 5, 6]. Zener drag force exerted by $M_{23}C_6$-type carbides precipitated on the lath boundaries is high enough to suppress their migration. The $M_{23}C_6$-type carbides give the major contribution to overall Zener drag pressure [5, 6] and, therefore, control stability of TMLS under creep conditions. It is well known [1, 2, 7] that a dispersion of M(C,N) carbonitrides plays an important role in creep resistance of high chromium martensitic steels. The service temperature of dilute 9Cr-Mo steel could be increased by 100 K owing to additional alloying by Nb and V [2]. It was assumed that the role of these carbontrides in creep strength of 9 %Cr steels consists in stabilization of TMLS under creep conditions [2, 7, 8]. However, analysis of Zener drag forces exerted by different kinds of dispersoids [5, 6] showed that the pinning pressure caused by $M_{23}C_6$ and even Laves phase precipitates is significantly higher than that exerted by the randomly distributed particles of (Nb,V)(C,N)-type carbonitrides. Such a minor increase in the pinning pressure by M(C,N) carbontrides could not be the main reason for extraordinary increase in creep strength of 9 %Cr martensitic steels. Therefore, these carbonitrides play the other important role in creep resistance of 9 %Cr steels.

✉ V. Dudko
valeriy_dudko@yahoo.com

[1] Belgorod State University, Pobeda 85, Belgorod, Russia 308015

The M(C,N) carbonitrides provide superior creep resistance due to superposition of two factors. First, these dispersoids play a role of effective agents for dispersion hardening inducing high threshold stress [9–13]. Second, M(C,N) carbontrides prevent the knitting reactions between lath boundaries and lattice dislocations [2]. The lath boundaries, which consists of irregular dislocation networks, exhibit long-range internal stresses and serve as effective obstacles to the dislocation motion [10, 14, 15]. However, the knitting reactions may lead to annihilation of dislocations with opposite signs that decreases the dislocation density [5, 6] and long-range stress fields originated from lath/subgrain boundaries [10], resulting in softening and lack of creep resistance [17]. Therefore, the structural strengthening attributed to the lath boundaries is one of the most important strengthening mechanisms of the 9 %Cr steels [2, 16, 17]. The aim of the present work is to clarify the role of M(C,N) carbonitrides in steady state creep behavior of a P92-type steel.

## 2 Materials and Methods

The P92-type steel with the chemical composition of Fe-0.1C–0.17Si–0.54Mn–8.75Cr–0.21Ni–0.51Mo–1.60W–0.23V–0.07Nb (all in wt%), was produced by Chelyabinsk Metallurgical Plant, Russia. This steel was solution treated at 1323 K and then tempered at 993 K for 3 h. Tensile specimens with a cross section of 7 × 3 $mm^2$ and gauge length of 25 mm were subjected to creep tests at 923 K under an initial stress from 118 to 200 MPa. Microstructural characterization was carried out using interrupted creep specimens by a Jeol JEM-2100 transmission electron microscope (TEM). The details of structural characterization are reported in previous works [5, 18, 19]. Misorientation of lath boundaries was determined using the conventional Kikuchi-line technique with TEM [20]. At least 50 boundaries were analyzed for each specimen. The small lattice curvatures within the individual laths/subgrains were evaluated from the rotation vector component in the plane of the electron diffraction pattern [21]. In addition, the internal stresses were examined by X-ray diffraction using a Rigaku Ultima IV diffractometer equipped with a CuKα radiation source [22].

## 3 Results

### 3.1 Initial Microstructure

The tempered martensite lath structure (TMLS) of the P92 steel is shown in Fig. 1a. The lath thickness and lattice dislocation density are 330 nm and 6.2 × $10^{14}$ $m^{-2}$, respectively. The average misorientation of lath boundaries is 2.7°.

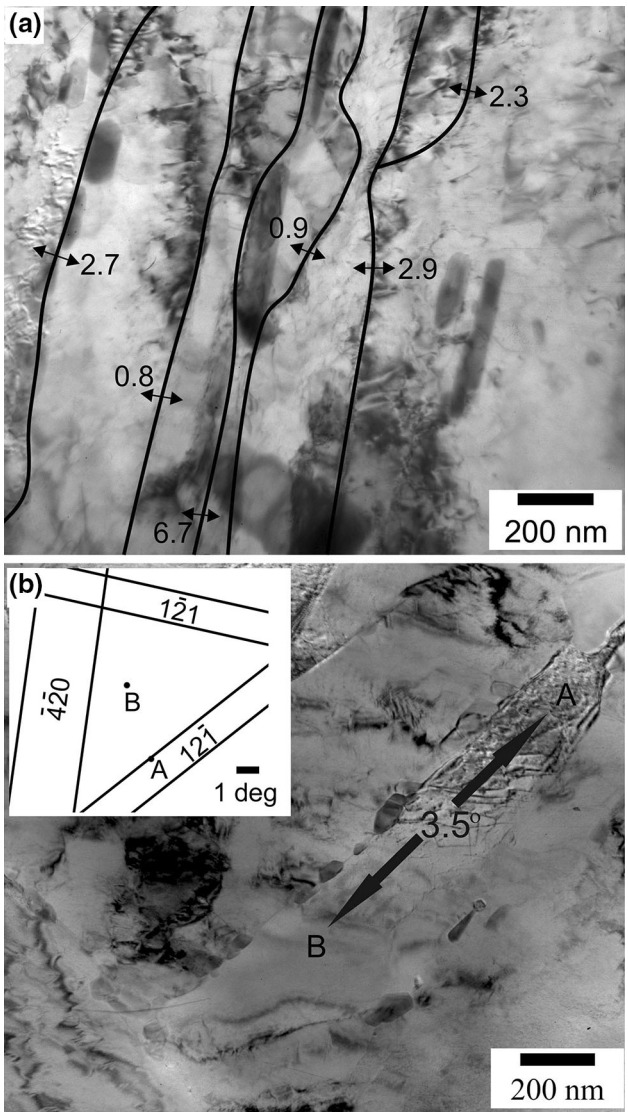


**Fig. 1** The TMLS of P92 steel after normalization at 1323 K followed by tempering at 993 K for 3 h (**a**) and lattice curvature within the lath (**b**)

A typical example of lattice curvatures is shown in Fig. 1b. The letters within the lath interior (i.e., A and B) indicate the local regions where the crystal lattice orientations were precisely determined. The Kikuchi diffraction patterns obtained from the lettered regions are schematically shown in the insert with A and B indicating the position of the central electron beam. The lattice curvature between these selected local regions can be roughly evaluated by measuring the distance between points A and B in the diffraction pattern [21, 23]. The residual shear stresses, $\tau$, associated with the maximal elastic distortion can then be calculated as follows [23]:

$$\frac{\tau_{lath}}{G} = \frac{0.35t\theta}{l}, \quad (1)$$

where $G$ is the shear modulus, $t$ is the foil thickness, $\theta$ is the angular disorientation between any two points within the lath, and $l$ is the distance between the measured points. The internal stresses were evaluated for 10 different laths and the average value was 75 MPa. Nearly the same value of 70 MPa was obtained by X-ray analysis.

### 3.2 Creep Behavior

The creep rate versus strain curves for applied stresses of 118, 140, 160, and 200 MPa are shown in Fig. 2a. The off-set strain, at which minimum creep rate is attained, increases from 2 to 4 % with decrease in applied stress from 200 to 140 MPa. The difference between the initial strain rate and the minimal strain rate also increases as applied stress decreases. On the other hand, at applied stress of 118 MPa, the off-set strain comprises 1 %. It is worth noting that decreasing the off-set strain with stress has been shown for the applied stress ≤140 and 923 K [24]. The minimal strain rate was taken as steady state creep rate [11]. Then, the creep behavior can be described by a power law between the stress and minimal strain rate [11]:

$$\dot{\varepsilon}_{\min} = A\sigma^{n*},$$

where $A$ is a constant, $n*$ is the apparent stress exponent. Figure 2 shows the dependence of minimal strain rate versus stress as plotted on double logarithmic scale (Fig. 2b).The creep behavior is characterized by relatively high apparent stress exponent, which tends to increase from 11 to 17 as $\sigma$ decreases from 200 to 118 MPa that is indicative of the presence of threshold stress [12, 13]. Therefore, the creep behavior is represented by the following relationship [10–13]:

$$\dot{\varepsilon}_{\min} = A(\sigma - \sigma_{th})^n$$

where $\sigma_{th}$ is the threshold stress, $n$ is the true stress exponent. The following procedure [12, 13] was used to determine the threshold stress. The experimental data were plotted as $\dot{\varepsilon}_{\min}^{1/n}$ against the steady state flow stress, $\sigma$, on double-linear scale with various n values (Fig. 2c) [12, 13]. It was found that the stress exponent of $n = 5.5$ yields the best linear fit. This value corresponds to the creep controlled by high temperature dislocation climb (lattice diffusion) [13]. Extrapolating this straight line to a zero strain rate yields a threshold stress value of 88 MPa.

### 3.3 Crept Microstructure

Evolution of TMLS at 118 MPa was considered in previous works [5, 10] in detail. The precipitation of Laves phase particles at boundaries, an increase (+20 %) in the size of $M_{23}C_6$ carbides and two-fold decrease in the lattice dislocation density take place during primary creep [5]. At the off-set strain of 1 %, the lath thickness, average misorientation of lath boundaries (Fig. 3) and dimensions of Nb- and V-rich M(C,N) carbonitrides remain unchanged. It is seen that transient creep increases curvature of lath boundaries (Fig. 3), which were straight after tempering (Fig. 1). It should also be noted that the internal stresses calculated by aforementioned TEM technique and X-Ray analysis decrease to 50 MPa. Decrease in the internal stress during primary creep can be attributed to two fold decrease in the dislocation density. Therefore, −30 % decrease in the internal stress is the main change of TMLS during transient creep.

## 4 Discussion

The threshold stress can be attributed to the presence of a dispersion of particles acting as effective barriers to mobile dislocations. In P92-type steels, the $M_{23}C_6$ and Laves

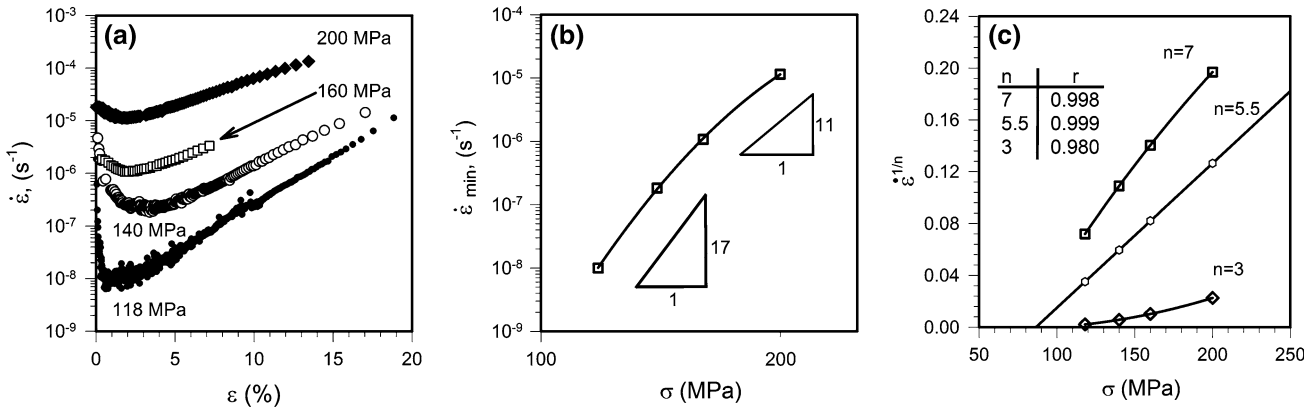


**Fig. 2** Creep behavior of the P92 steel at 923 K. The regression coefficients (r) of linear approximations for different stress exponents (n) are shown in the *inset* (**c**)

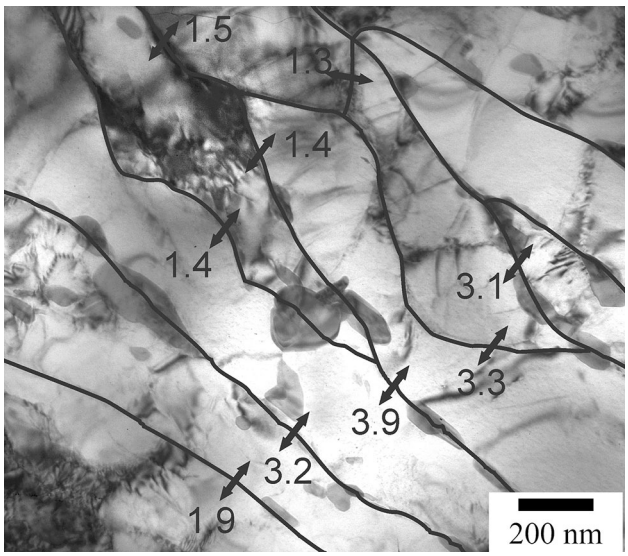


**Fig. 3** The microstructure of the P92 steel after 1 % creep at 923 K

phase particles mostly precipitate at various boundaries and could not serve as obstacles to moving dislocations. Therefore, the threshold stresses can originate from M(C,N) particles, which are distributed mainly within laths [10]. Several models were developed to explain threshold stress [12, 13]. These models compare the threshold stress with the stress required to (a) bow a dislocation between two particles (Orowan stress), (b) create the additional dislocation segment as a dislocation surmounts an obstacle by local climb, (c) detach a dislocation from an attractive particle after climb is completed. Orowan stress, $\tau_O$, could be evaluated by the following equation [13]:

$$\tau_O = 0.84\,Gb/(\lambda - d), \tag{2}$$

where $\lambda$ is the interparticle distance, and $d$ is the particle size. The extra back stress, $\tau_b$, required to generate sufficient additional dislocation length to climb over an obstacle could be derived from the following equation [13]:

$$\tau_b = 0.3\,Gb/\lambda \tag{3}$$

The detachment stress, $\tau_d$, required to break the dislocation from the particle after the climb has finished is calculated by the following equation [13]:

$$\tau_d = Gb\left(1 - K^2\right)^{1/2}/\lambda, \tag{4}$$

where $K$ is a relaxation parameter. The following parameters were used to calculate the theoretical values of $\tau_O$, $\tau_b$ and $\tau_d$: $G = 60$ GPa at 650 °C, $b = 2.48 \times 10^{-10}$ m. The planar spacing between particles is $\lambda = 0.5d(\pi/(6F_v))^{0.5}$ [25], where $F_v$ is the volume fraction of the MX particles and $d$ is the average MX particle size, which were taken as 0.23 % and 31 nm, respectively.The magnitudes of the theoretical threshold stresses are summarized in Table 1 along with the experimental values for the threshold and internal stresses. A relaxation parameter, $K$, was assumed to be 0.6 [10]. It should be noted that the exact magnitude of the relaxation parameter cannot be estimated because of the numerous assumptions and approximations used during theoretical treatments [13]. A low relaxation parameter of 0.6 was chosen to provide the best match to the experimental data. However, numerous studies on detachment stresses have reported $K$ values of more than 0.8 [13]. Therefore, the real operating detachment stress should be less than those presented in Table 1.

The Orowan stress, the detachment stress and the internal stresses are almost the same. It is unlikely that the local climb can be related to threshold stress since $\tau_b$, value is about three-fold lower. Therefore, both the dispersion of M(C,N) carbonitrides, which leads to Orowan stress or detachment stress, and the internal stresses, which are attributed to the dislocation substructure, can exert the threshold stress in the P92 steel [10–15]. The dispersion and structural hardening are responsible for the extraordinary high creep resistance of P92-type steels. In both cases, the M(C,N) dispersoids play an important role. First, the carbonitrides contribute directly to creep resistance by exerting the threshold stress being slightly higher than allowable stress for P92 steel at 650 °C [26]. The dispersion hardening mechanism is realized through threshold behavior. Second, M(C,N) carbontrides slow down the aforementioned knitting reaction and internal stress retains at sufficiently high level after termination of transient creep. As a result, the structural strengthening attributed to fine lath thickness and internal stress originated from these boundaries plays an important role in steady state creep behavior. Namely, the threshold stresses associated with a dispersion of M(C,N) particles through two different hardening mechanisms provide superior creep resistance of 9 %Cr steels.

**Table 1** Measured microstructural parameters, theoretical values of Orowan stress ($\tau_O$), extra back stress ($\tau_b$) detachment stress ($\tau_d$), internal stresses ($\tau_{lath}$ (TEM), $\tau_{lath}$ (X-Ray)) and threshold stresses ($\tau_{th}$) (MPa) in P92 steel

| ε (%) | $d$ (nm) | $\theta/l$ ($10^{-5}$ nm$^{-1}$) | $\tau_O$ | $\tau_b$ | $\tau_d$ | $\tau_{lath}$ (TEM) | $\tau_{lath}$ (X-Ray) | $\tau_{th}$ |
|---|---|---|---|---|---|---|---|---|
| | | Equation 1 | Equation 2 | Equation 3 | Equation 4 | Equation 1 | $\tau_{X\text{-}Ray}$ | $\sigma_{th}/\sqrt{3}$ |
| 0 | 31 | 2.8 | 62 | 19 | 51 | 76 | 66 | – |
| 1 | 31 | 1.8 | 62 | 19 | 51 | 49 | 47 | 51 |

## 5 Conclusions

1. An average lath size of 330 nm and dislocation density of $6.2 \times 10^{14}$ $m^{-2}$ within the lath were obtained for P92 steel after tempering at 993 K for 3 h. The tempered structure was characterised by large curvatures in the lath lattice, which resulted in internal stresses of 75 MPa. The average misorientation of the lath boundaries was $\sim 2.5°$.
2. At 933 K and an applied stress of 118 MPa, the transient creep led to insignificant growth of boundary particles and two-fold decrease in the lattice dislocation density. The internal stress decreased from $\sim 75$ to $\sim 50$ MPa.
3. At applied stress ranging from 118 to 200 MPa, the P92 steels exhibited threshold behavior. The stress exponent increases from 11 in the strain rate range from $10^{-6}$–$10^{-5}$ $s^{-1}$ to 17 in the range from $10^{-8}$–$10^{-7}$ $s^{-1}$, which suggests a threshold stress of $\sim 50$ MPa.
4. Theoretical analysis showed that the internal stress, Orowan bowing and detachment of lattice dislocations from dispersoids may induce the threshold stress.

**Acknowledgments** The study was financial supported by the Russian Science Foundation, under Grant No. 14-29-00173. The authors are grateful to the staff of the Joint Research Center, Belgorod State University, for their assistance with instrumental analysis.

## References

1. Maruyama K, Sawada K, and Koike J, *ISIJ Int* **41** (2001) 641.
2. Abe F, in *Creep-Resistant Steels*, (ed) Abe F, Kern T-U, Viswanathan R, Woodhead publishing ltd., Cambridge (2008), p 279.
3. Hald J, *Int J PresVes Pip* **85** (2008) 30.
4. Abe F, Horiuchi T, Taneike M, and Sawada K, *Mater Sci Eng A* **A378** (2004) 299.
5. Dudko V, Belyakov A, Molodov D, and Kaibyshev R, *Metall Mater Trans A* **44** (2013) 162.
6. Dudova N, Plotnikova A, Molodov D, Belyakov A, and Kaibyshev R, *Mater Sci Eng A* **534** (2012) 632.
7. Taneike M, Abe F, and Sawada K, *Nature* **424** (2003) 294.
8. Kostka A, Tak K-G, Hellmig R J, Estrin Y, and Eggeler G, *Acta Mater* **55** (2007) 539.
9. Spigarelli S, Cerri E, Bianchi P, and Evangelista E, *Mater Sci Techn* **15** (1999) 1433.
10. Dudko V A, Belyakov A N, and Kaibyshev R O, *Dokl Phys Chem* **464** (2015) 191.
11. Kassner M E, and Pérez-Prado M T, *Fundamentals of Creep in Metals and Alloys 1st ed*, Elsevier, Amsterdam (2004).
12. Kaibyshev R, Musin F, Avtokratova E, and Motohashi Y, *Mater Sci Eng A* **392**, (2005) 373.
13. Mohamed F A, Park K-T, and Lavernia E J, *Mater Sci Eng A* **150**, (1992) 21.
14. Sedlacek R, Blum W, Kratochvil J, and Forest S, *Metall Mater Trans* A **33** (2002) 319.
15. Straub S, Blum W, Maierz H J, Ungar T, Borbely A, and Renner H, *Acta Metall Mater* **44** (1996) 4337.
16. Abe F, *Mater Sci Eng A* **510–511** (2009) 64.
17. Ghassemi-Armaki H, Chen R P, Maruyama K, and Igarashi M, *J Nucl Mater* **433** (2013) 23.
18. Fedoseeva A E, Kozlov P A, Dudko V A, Skorobogatykh V N, Shchenkova I A, and Kaibyshev RO, *Phys Met Metall* **116** (2015) 1047.
19. Dudko V A, Fedoseeva A E, Belyakov A N, Kaibyshev R O, *Phys Met Metall* **116** (2015) 1165.
20. Zaefferer S, *Adv Imaging Electron Phys* **125** (2002) 355.
21. Belyakov A, Sakai T, Miura H, and Kaibyshev R, *Phil Mag Let* **80** (2000) 711.
22. He B B, *Two-Dimensional X-ray Diffraction*, Wiley, Hoboken (2009).
23. Belyakov A, Tsuzaki K, Kimura Y, and Mishima Y, *Phil Mag Let* **89** (2009) 201.
24. Kimura K, Sawada K, Kushima H, and Kubo K, *Int J Mat Res* **99** (2008) 395.
25. Humphreys F J, Hatherly M, *Recrystallization and Related Annealing Phenomena*. 2nd ed, Elsevier, UK (2004).
26. Yoshizawa M, Igarashi M, Moriguchi K, Iseda A, Armaki H, G, and Maruyama K, *Mater Sci Eng A* **510–511** (2009) 162.